Impact of Duodenal Image Capturing Techniques and Duodenal Regions on the Performance of Automated Diagnosis of Celiac Disease

S.Hegenbart, R.Kwitt, M.Liedlgruber, A.Uhl
Department of Computer Sciences
Salzburg University, Austria

A.Vécsei
St. Anna Children's Hospital
Vienna, Austria

Abstract

Various techniques have been developed for an automated classification of endoscopic images. Besides the classical methods for endoscopic image capturing, new methods like the modified immersion technique have been devised and are in use. The impact of specific image capturing techniques for feature extraction and classification in automated diagnosis is unclear. This work applies several well tested methods for feature extraction and classification on images captured with the conventional and the modified immersion technique. We compare the classification rates and the impact on feature extraction of each specific capturing technique. We also compare the classification rates of different duodenal regions. Finally we advise an optimal combination of image capturing technique, duodenal region and feature extraction methods for automated celiac disease diagnosis.

1. Introduction

Esophagogastroduodenoscopy (EGD) followed by multiple biopsies is currently the gold standard for celiac diagnosis. Optimal targeting of duodenal biopsies is not trivial. Automated Classification in a medical context can be used as a support tool for the physician. Methods that help indicating specific areas for biopsy might improve the reliability of celiac disease diagnosis.

Multiple types of endoscopic image capturing techniques exist. We compare the efficiency of classification of images captured by two major imaging techniques, the modified immersion and the conventional technique. Besides the difference through capturing, the images also vary, depending on the region of the duodenum that is shown. This work uses multiple well tested feature extraction and classification methods that proved feasible in medical pattern recognition. The efficiency of classification of the two image capturing techniques and the two duodenal regions is compared. Also a discussion of possible problems related to the different image types is given. Additionally we define celiac markers within images that worked best for feature extraction and classification.

1.1 Automated classification

When implemented as a support tool for the physician, the classification process has to be fully automated. The automated process consists of three major steps. The first vital step is deciding on one or more image regions for extraction that are most representative for the specific classification problem. We discuss this step in further detail in Section 2.3. The next step deals with improving the extracted region's quality by applying image processing techniques. We discuss preprocessing options in Section 3. In the last step the discriminative information of the extracted region for each image is encoded as a numerical feature vector. Using these feature vectors, each classifier's optimal parameters are then estimated. Any unknown feature vector is finally classified by using the estimated parameters.

2. Image acquisition and preparation

The data set we used for testing consists of images from two distinct regions of the duodenum (the bulbus duodeni and pars descendes). The images were taken at the St. Anna's Children Hospital using a standard duodenoscope without magnification. The celiac state of the images was determined by visual inspection during the endoscopy session followed by a biopsy of suspicious areas. Through a histological examination of the mucosal state of the extracted tissue the severity of the villous atrophy was defined according to Marsh classification. For each patient, beside the classical endoscopy technique a new endoscopic approach, the modified immersion technique, for diagnosing celiac disease was applied.

The captured image data was manually inspected and filtered by several qualitative factors (sharpness, distortions, visibility of features). As the final step, image regions with a high specificity for celiac disease, or absence of celiac disease were extracted. More than half of the images had to be discarded because they did not satisfy the qualitative specifications.

2.1 Image capturing techniques

For the endoscopy procedure the patient swallows a small flexible tube called an endoscope. The endoscope

transmits a video stream through a data channel to the physician. The scope is able to insert air and water to expand existing folds and structures. The conventional image capturing technique involves no special treatment of the small bowel. A standard camera for duodenoscopy is used. In contrast, the modified immersion technique is based on the instillation of water into the duodenal lumen for better visualization of the villi. The camera is then put into the water, and images of interesting areas are taken. Studies [3] show that visualization of villi with the immersion technique has a higher positive predictive value.

2.2 Celiac specific markers

Several endoscopic markers indicating celiac disease exist. Not all show great promise for automatic classification. It is important to identify frequent and robust markers. As stated in [2] markers include mosaic or nodular mucosa, scalloping of duodenal folds and reduction in number or even absence of duodenal folds (Kerckring's folds). The sensitivity of endoscopic markers is highly variable because of their absence through a possibly lower degree of villous atrophy. Visible villi structures usually indicate a normal mucosal state. However a symptom described as patchy villous atrophy exists, where only parts of the mucosa are affected and show a reduced number or absence of villi. Hence in automated classification an image region classified as no celiac is not sufficient to classify the patient as healthy. Our research shows that the villi structure and the mosaic or nodular mucosa work best as markers for classification purposes.

2.3 Duodenal regions and their impact on image quality and homogeneity

Endoscopic images show a high variance with respect to sharpness and degree of existent distortions. The bowel resembles a tube, as a side effect the chosen perspective changes considerably among images. This leads to problems, especially within the pars descendens region. Results show that the extracted image region plays a crucial role in the classification of endoscopic images. The duodenum is divided into two parts. The bulbus duodeni and the pars descendens regions. Textures within images from the bulbus region lie in the tangent plane to the surface. This is a result of the "flat" form of the bulb. The pars descendens region shows many duodenal folds. The villi texture within the pars descendens region varies between a tangential orientation to a perspective that points out of the surface of the image.

The uniform texture orientation within the bulbus leads to a higher degree of homogeneity across the images, nevertheless markers like the scalloping of folds or the reduction in number of folds are not visible in this area. In automated classification the homogeneity in perspective across the images is a big advantage and current results show better classification rates for images from the bulbus region.

Beside villi structures, the folds presented within the pars descendens show indicators whether the tissue is affected of celiac disease or not. While manual inspection of this area might provide better classification results, automated classification faces a couple of problems when working with images taken from this region. Markers like scalloping or reduction in number of folds can not be efficiently represented and extracted within a frequency spectrum. Also the anatomic form of the pars descendens is problematic. For better visibility of celiac markers present on the folds, the physicians change the camera's perspective frequently and hence the textural orientation changes. This causes inhomogeneities within the image test sets.

2.4 Image-Region extraction

Not all duodenal image regions show a high specificity for celiac disease. Even more, only parts of a celiac small bowel might be affected of villous atrophy. This indicates that it is of high priority to extract an image region with the highest specificity. In automatic image-region extraction, qualitative indicators such as image-blur and image-distortions could be used to decide on optimal regions. Methods used within content-based image retrieval might be applicable here. The relations between eigenvalues of the windowed image second moment as described in [1] could be used as an indicator for specific textural regions. In this project, the step was performed manually, as automated techniques that deal with choosing appropriate regions are still subject to further research.

Beside the location of the chosen regions within an image its size plays a crucial role. For classification this size is fixed within a test set. Larger regions do contain more specific markers, but also tend to be of lower quality, as the perspective is more static and distortions are harder to avoid. Also the accuracy of diagnosis suffers from a larger region size (patchy villous atrophy). We chose square image regions with 256×256 pixels of length for extraction in the bulbus region. This size proved to be too large for the pars descendens region. The perspective within the pars descendens limits the size of the extracted square. Results show, that features extracted from 256×256 pixel squares are not discriminative enough. Methods using some sort of feature subset selection or evolutionary optimization tend to overtrain the classificators and lead to invalid results. To avoid this problem, we decided to use squares with the length of 128×128 pixels. Figure 1 gives an intuitive comparison of the 256×256 pixel region with the 128×128 pixel region for an image from the pars descendens.

2.4.1 Perspective and zoom

The perspective plays a significant role in choosing an appropriate region of the image for classification. The classification performance is tied to the visibility of a set of features. As mentioned in Section 2.3 the interesting part of the mucosa of the bulbus duodeni is flat. Pictures from this region only differ in the zoom scale. On the other hand,

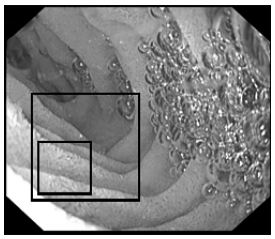

Figure 1. Impact of image region size

the pars descendens region is characterized by its form resembling a tube. Images from this region differ heavily in the form of visible features. Images with a frontal perspective and high zoom show features comparable to the bulbus images. For capturing features visible on top of the folds (e.g. villi structure or scalloping) a lateral perspective is superior to a frontal perspective. Although the features are the same, the perspective might fool the classification process. The feature extraction method must be capable of dealing with differing zoom scales. Images that were captured at a low zoom level usually lose quality in visibility of tissue structure.

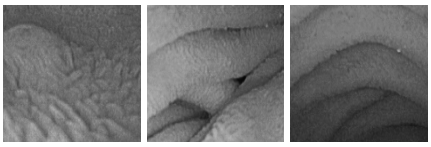

Figure 2. Images from the pars descendens with changing perspective and zoom

2.4.2 Distortions

Most images show regions with a high density of small bubbles. This effect was observed more often in images that were captured using the conventional method. The modified immersion technique is based on the instillation of water into the duodenal lumen. As a benefiting side effect, no bubbles are below the surface of water and this type of distortions is less likely to obscure important features. The instillation of water poses an interesting phenomenon. Most pictures (depending on the perspective) show a mirrored version of the captured area at the water surface. This has not been a problem yet. Even more its redundancy might be even helpful in automated region extraction. Light reflections can be frequently observed on the moist tissue, especially when the images were captured conventionally. The way the tissue reflects the lights might also be an indicator for celiac disease. But there has not been any research on this topic yet.

2.4.3 Blur and exposure

Most endoscopic images are partially blurred. This effect is a result of the lens losing its focus. This causes the captured

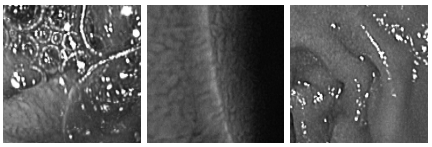

Figure 3. Images with distortions

image to suffer from a loss in sharpness. Blurred tissue regions resemble regions without structural information. Care has to be taken not to confuse the blurred villi structure with the absence of villi structure (indicating celiac disease). A way to avoid using blurred regions, is an algorithm that provides a measure for existing blur. As proposed in [9] the spread of edges could be used to identify blurred regions. Beside blurred regions suboptimal exposure is unavoidable. Long exposures lead to motion blur, while short exposures require very good lighting of the specific area. Underexposed images can be very noisy. This must not be interpreted as existing villi structure. A way to handle uneven exposure is a local contrast and histogram equalization.

Figure 4. Images with partial blur and suboptimal exposure

3. Preprocessing

High image quality is crucial for a good classification performance. To improve the performance we applied an advanced contrast enhancement technique called CLAHE (Contrast Limited Adaptive Histogram Equalization) [10] on a slightly blurred version of the extracted region. The blurring process uses a Gaussian blur filter with a small (2x2) kernel. The final step is a sharpening of the image using Laplace sharpening. To avoid highlighting present noise, we used a rather large (9x9) kernel for sharpening.

4. Feature extraction and classification

Many well tested methods for feature extraction exist. To gain a comprehensive view on how the classifications of different image types perform, we applied several feature extraction methods that led to promising results in medical pattern recognition in other works. We used the following feature extraction and classification methods:

- *FFT-kNN* Evolutionary Feature Selection, Classic features. [10] The FFT is used to transform the image into it's frequency spectrum. Multiple ring shaped filters are then applied to the Fourier spectrum of each

color channel to select relevant subsets of the most discriminative coefficients. The feature vectors are then classified by a k-NN classification using the Euclidean distance.

- *FFT-Bayes* Evolutionary Feature Selection, Classic features. [10] Same as above, using a statistical Bayes classifier for classification.

- *FFT-SVM* Evolutionary Feature Selection, Classic features. [10] Same as above, using a non-linear SVM classifier with radial basis function as kernel ($K(x_i, x_j) = e^{-\gamma|x_i - x_j|^2}$).

- *DT-CWT, Weibull* Dual-Tree Complex Wavelet Transform, 6 scales, Weibull features [5]. The DT-CWT is used to decompose the images. The empirical histogram of the detail subband coefficient magnitudes is modelled by two-parameter Weibull distributions. The Weibull parameters are then arranged into a feature vector and the Euclidean metric is used for 1-NN classification.

- *DT-CWT, Classic* Dual-Tree Complex Wavelet Transform, 6 scales, Classic features [5, 8]. The DT-CWT is used to decompose the images. Features are computed from the mean and standard deviation of the absolute values of the complex detail subband coefficients. This is the same setup as it is used in [8], except that we use the DT-CWT instead of the Gabor Wavelet Transform. The classification is performed by a 1-NN classification using the Euclidean metric.

- *DWT, Classic* Pyramidal Wavelet Transform, 6 scales, Weibull features [8]. Same features are extracted as in [5], but the classic pyramidal wavelet transform is applied. The features are classified by a 1-NN classification using the Euclidean metric.

- *Gabor, Classic* Gabor Wavelet Transform, 4 scales, 6 orientations, Classic features [8]. The features are classified by a 1-NN classification using the Euclidean metric.

- *DWT-ES*, Pyramidal Wavelet Transform, 6 scales, Eigen Subband features [6]. Eigen Subbands are computed from the stacked Wavelet detail subbands at equal positions in the decomposition structure of each color channel. The corresponding Eigenvalues are arranged in a feature vector which is then used for 1-NN classification using the Euclidean metric.

- *DT-CWT, ES* Dual-Tree Complex Wavelet Transform, 6 scales, Eigen Subband features [6]. The features are classified by a 1-NN classification using the Euclidean metric.

- *SWT-ES*, Stationary Wavelet Transform (á trous), 6 scales, Eigen Subband features [6]. The features are classified by a 1-NN classification using the Euclidean metric.

- *LDB-WT*, Wavelet Decomposition Depth 3, Subband Energy (over all coefficients) as features [7]. The Local Discriminant Basis algorithm is employed to find an optimal Wavelet decomposition basis with respect to discrimination between the image classes. After transforming all images into this basis, for each of the resulting subbands the energy over all coefficients is computed for each color channel separately. The energy values of all channels are then concatenated to form the feature vectors, which are used in conjunction with the 1-NN classifier for the classification.

- *GMRF-WT*, Gaussian Markov Random Fields, Pyramidal Wavelet transform, Wavelet Decomposition Depth 2, Geman neighbourhood of order 5 [4].

  The Pyramidal Discrete Wavelet Transform is used to decompose the images. For the resulting subbands the Markov parameters are estimated for each color channel separately, using a Geman neighbourhood of order 5. The concatenated parameters are subsequently used as feature vectors for the classification by using a Bayes classifier.

- *WTP-SE*, Pyramidal Wavelet Transform, Decomposition Depth 5, Subband Energy (over all coefficients) as features [7]. The wavelet subbands are used to compute the energy over all coefficients within the subband, which is done for each color channel separately. The energies of all subbands and color channels are then concatenated and used for the classification using the Bayes classifier.

4.1 Multiclassification

Apart from using the methods described in Section 4, we combine the best methods using a multiclassifier. This classifier is based on a reliability measure for each single method, taking into account its classification rate (described in more detail in [10]). Using the multiclassifier we seek an optimal combination of methods and the according parameters, with the goal of obtaining a better overall classification rate.

5. Experimental setup

Our experimental tests distinguish between images captured with the new modified immersion technique and the conventional technique. The tests are conducted separately on images from the bulbus and the pars descendens regions. The parameter set for each classifier was first computed by the methods described in Section 4 by using the leave-one-out cross validation protocol. This was performed separately for each duodenal region and imaging technique. The final results reflect each method's performance in a leave-one-out cross validation. Table 1 lists the distribution of images within the test sets.

	No Celiac	Celiac	Total
Bulbus Immersion	264	121	385
Bulbus Conventional	116	34	150
Pars Immersion	183	197	380
Pars Conventional	49	35	84

Table 1. Distribution of image data

6. Results

Only results with an overall classification rate better than 80% (for the bulbus) and 73% (for the pars descendens) are included in the tables. Not all methods are feasible on grayscale and color images, hence a missing method does not necessarily indicate a rate below the chosen thresholds. Grayscale and color refer to whether the features are extracted from each colorchannel separately or from a grayscale version of the image. The presented numbers are the percentages of correctly classified images together with their specificity and sensitivity (TNR and TPR).

TNR indicates the method's specificity (True Negative Rate) i.e. the percentage of correctly classified images actually showing a normal mucosal state, TPR denotes the sensitivity (True Positive Rate) i.e. the percentage of correctly classified images showing villous atrophy.

Table 2 shows the results of the specific methods for the bulbus region. We see, that features extracted from the color space have a slight advantage over grayscale features. When comparing single methods, both feature extraction spaces seem feasible.

Images from the set captured with the immersion technique have an advantage in classification rate over the classical images. The difference in the bulbus region is between 1.4% and 9.9% total percentage points. The sensitivity was considerably higher for all methods classifying the immersion images from the bulbus, while the specificity did not show a big difference among the image capturing techniques.

The best classification rates were achieved by the Fourier methods. This can be explained by the additional feature set optimization that took place during the evolutionary optimization of its ring-shaped filters. However this optimization poses the risk of overtraining the classifier when small unbalanced image sets are present. Features from the Dual Tree Wavelet Transform and Markov Random Fields perform comparably to the Fourier methods, even without feature set optimization.

Table 3 presents the classification results of images from the pars descendens region. Again both feature spaces provide similar results. As expected, the inhomogeneities within the test set result in a lower classification rate compared to the bulbus test set, of about 8.5% total percentage points for immersion and 15% total percentage points for conventional images. The difference between immersion and conventional images is also present within the pars descendens. Classification of the immersion set performs 0.5% to 21% total percentage points better. It is interesting that the worse total classification rates compared to the bulbus are caused by a decrease of specificity. The sensitivity was stable among the two duodenal regions. The features extracted from the Dual Tree Wavelet Transform space perform comparably to the Fourier methods again in the pars descendens. On the other hand Markov Random Field methods perform worse, compared to the bulbus region.

6.1 Results of multiclassification

Tables 2 and 3 show the results by combining the best methods in the subsection Multiclassification. We searched the best combination of methods for each image region and capturing technique. The results that were used for the specific multiclassifiers are shown in bold in Tables 2 and 3. Each image type and image region was classified separately.

Multiclassification improved the classification rate of images from the bulbus by 3% total percentage points for immersion and 4% total percentage points for conventional. Immersion images still have a slight advantage over conventional images in the bulbus. The results correspond to the results of the single methods.

The multiclassification of the pars descendens improved the classification rate by 4% total percentage points for the immersion and 8% total percentage points for the conventional images. It is interesting that the multiclassification of the conventional pars descendens images returned a result with a superior conventional rate of 3% total percentage points compared to the immersion images. This is remarkable as most single classification methods performed better for the immersion image type.

Our analysis of the results showed some interesting facts. As shown in Table 1 the image set of the conventional images from the pars descendens is considerably smaller than the immersion image set of the pars descendens. A single conventional image that was correctly classified by the multiclassification had a significant impact of 1.2% total percentage points, compared to only 0.26% total percentage points for the immersion images.

A high diversity among base classifiers is a necessary condition for an improvement in the ensemble performance. The diversity gives a measure how correlated classification outcomes of the single methods are. We applied several standard diversity measures to analyze our methods. As a result the mean diversity among the classifiers of the immersion images was only half compared to the conventional images. Beside that, the base classifiers' reliabilities were lower for the conventional images of the pars descendens. This caused a decrease in the classification rate of 10% total percentage points when a highly non-linear version of the remapping function (controlling how strong the reliability of a method influences the result of the multiclassifier) as explained in [10] was used.

The high diversity combined with the small image set led to the effect, that the multiclassification yields significantly better classification rates than the single methods for the conventional images from the pars descendens.

Method	Bulbus Immersion			Bulbus Conventional		
	TNR	TPR	Total	TNR	TPR	Total
Color Features						
FFT-SVM	**96.67**	**85.00**	**93.24**	**93.97**	**70.59**	**88.66**
FFT-Bayes	**92.42**	**89.17**	**91.42**	**94.83**	**73.53**	**90.00**
FFT-kNN	**95.83**	**86.67**	**92.80**	**95.68**	**58.80**	**87.33**
DT-CWT, Weibull	**90.15**	**79.17**	**86.72**	85.34	50.00	77.33
DT-CWT, Classic	**92.80**	**87.50**	**91.15**	**88.79**	**55.88**	**81.33**
DT-CWT, ES	86.36	77.50	83.59	88.79	44.12	78.67
DWT, Classic	87.88	74.17	83.59	92.24	64.71	86.00
DWT-ES	82.20	76.67	80.47	85.34	47.06	76.67
SWT-ES	83.33	73.33	80.21	84.48	47.06	76.00
Gabor, Classic	90.91	85.83	89.32	89.66	50.00	80.67
GMRF-WT	**92.05**	**85.00**	**89.84**	91.38	58.82	84.00
LDB-WT	87.88	77.50	84.63	**91.38**	**64.71**	**85.33**
WTP-SE	**94.32**	**75.00**	**88.28**	93.10	55.88	84.66
Grayscale Features						
DT-CWT, Weibull	89.02	77.50	85.42	87.93	58.82	81.33
DT-CWT, Classic	94.32	78.33	89.32	91.38	52.94	82.67
DWT, Classic	89.39	75.83	85.16	84.48	47.06	76.00
Gabor, Classic	91.29	82.50	88.54	84.48	58.82	78.66
Multiclassification						
Multiclassifier	98.11	90.00	95.57	99.14	76.47	94.00

Table 2. Overall bulbus classification performance. The results of the methods used for the multiclassifier are shown in bold.

Method	Pars Immersion			Pars Conventional		
	TNR	TPR	Total	TNR	TPR	Total
Color Features						
FFT-SVM	**81.42**	**83.76**	**82.63**	**87.50**	**79.41**	**84.14**
FFT-Bayes	**84.70**	**82.23**	**83.42**	**87.50**	**76.47**	**82.93**
FFT-kNN	79.78	84.77	82.36	**72.92**	**85.29**	**78.05**
DT-CWT, Weibull	**78.14**	**83.25**	**80.79**	68.75	47.06	59.76
DT-CWT, Classic	**82.51**	**82.74**	**82.63**	64.58	52.94	59.76
DWT-ES	68.85	77.66	73.42	62.50	55.88	59.76
Gabor, Classic	78.69	82.74	80.79	60.42	61.76	60.98
LDB-WT	**62.84**	**82.74**	**73.15**	68.75	55.88	63.41
WTP-SE	80.33	69.04	74.47	45.83	91.18	64.63
Grayscale Features						
DT-CWT, Weibull	**74.86**	**87.31**	**81.32**	79.17	41.18	63.42
DT-CWT, Classic	76.50	78.17	77.37	77.08	55.88	68.29
DWT, Classic	73.77	79.70	76.84	68.75	64.71	67.07
Gabor, Classic	75.96	78.68	77.37	64.58	58.82	62.20
Multiclassification						
Multiclassifier	84.15	92.39	88.42	91.67	91.18	91.46

Table 3. Overall pars descendens classification performance. The results of the methods used for the multiclassifier are shown in bold.

7. Conclusion

Our results show that the detection performance of villous atrophy in duodenal images by an automated classification is heavily dependent on several factors. Beside the image capturing technique also the way distortions are handled and regions extracted play a big role. Our results show that the size of the extracted image region of 256×256 pixels is not adequate for both regions. Varying texture orientation and zoom scales can not be compensated by smart region extraction within the pars descendens. We advise to use a 128×128 pixel region for classifying images from the pars descendens region, while both 256×256 pixel and 128×128 pixel regions seem adequate for the bulbus.

Comparing the image capturing techniques, the modified immersion technique is superior to the conventional technique. Beside the better classification rate, the overall image quality and utility for classification is superior to the conventional technique as well. We achieved the best results by using images from the duodenal bulb using the modified immersion technique. Features from the Dual Tree Wavelet Transform, the Fourier Transform and Markov Random Fields gave the most promising results. This results could be further improved by combining several methods into a multiclassifier.

References

[1] S. Belongie, C. Carson, H. Greenspan, and J. Malik, "Region-based image querying", Technical Report UCB/CSD-97-941, EECS Department, University of California, Berkeley, Apr 1997.

[2] W. Dickey and D. Hughes, "Prevalence of celiac disease and its endoscopic markers among patients having routine upper gastrointestinal endoscopy", *American Journal of Gastroenterology*, 94, Aug. 1999, pp. 2182–2186.

[3] A. Gasbarrini, V. Ojetti, L. Cuoco, G. Cammarota, A. Migneco, A. Armuzzi, P. Pola, and G. Gasbarrini, "Lack of endoscopic visualization of intestinal villi with the immersion technique in overt atrophic celiac disease", *Gastrointestinal endoscopy*, 57, Mar. 2003, pp. 348–351.

[4] M. Haefner, A. Gangl, M. Liedlgruber, A. Uhl, A. Vécsei, and F. Wrba, "Combining gaussian markov random fields with the discrete wavelet transform for endoscopic image classification", In *Proceedings of the 17th International Conference on Digital Signal Processing (DSP'09)*, Santorini, Greece, 2009. to appear.

[5] R. Kwitt and A. Uhl, "Modeling the Marginal Distributions of Complex Wavelet Coefficient Magnitudes for the Classification of Zoom-Endoscopy Images", In *Proceedings of the IEEE Computer Society Workshop on Mathematical Methods in Biomedical Image Analysis (MMBIA'07)*, Rio de Janeiro, Brasil, 2007.

[6] R. Kwitt and A. Uhl, "Color Eigen-Subband Features for Endoscopy Image Classification.", In *Proceedings of the 33rd IEEE International Conference on Acoustics, Speech and Signal Processing (ICASSP 2008)*, pp. 589–592, Las Vegas, Nevada, USA, 2008.

[7] M. Liedlgruber and A. Uhl, "Statistical and structural wavelet packet features for pit pattern classification in zoom-endoscopic colon images", In P. Dondon, V. Mladenov, S. Impedovo, and S. Cepisca, editors, *Proceedings of the 7th WSEAS International Conference on Wavelet Analysis & Multirate Systems (WAMUS'07)*, pp. 147–152, Arcachon, France, Oct. 2007.

[8] B. S. Manjunath and W. Y. Ma, "Texture features for browsing and retrieval of image data", *IEEE Trans. Pattern Anal. Mach. Intell.*, 18(8), 1996, pp. 837–842.

[9] P. Marziliano, F. Dufaux, S. Winkler, T. Ebrahimi, and G. Sa, "A no-reference perceptual blur metric", In *IEEE 2002 International Conference on Image Processing*, pp. 57–60, Rochester, New York, 2002.

[10] A. Vécsei, T. Fuhrmann, M. Liedlgruber, L. Brunauer, H. Payer, and A. Uhl, "Automated classification of duodenal imagery in celiac disease using evolved fourier feature vectors.", *Comput Methods Programs Biomed*, Apr 2009.